ACS APPLIED MATERIALS & INTERFACES

Research Article

www.acsami.org

Cascading Boost Effect on the Capacity of Nitrogen-Doped Graphene Sheets for Li- and Na-Ion Batteries

Lei-Lei Tian,[†,‡] Si-Bai Li,[†,‡] Ming-Jian Zhang,[‡] Shuan-Kui Li,[‡] Ling-Piao Lin,[‡] Jia-Xin Zheng,[*,‡] Quan-Chao Zhuang,[*,§] Khalil Amine,[‡,⊥] and Feng Pan[*,‡]

[‡]School of Advanced Materials, Peking University, Shenzhen Graduate School, Shenzhen 518055, China

[§]School of Materials Science and Engineering, China University of Mining & Technology, Xuzhou 221116, China

[⊥]Electrochemical Technology Program, Chemical Sciences and Engineering Division, Argonne National Laboratory, Argonne, Illinois 60439, United States

Supporting Information

ABSTRACT: Specific capacity and cyclic performance are critically important for the electrode materials of rechargeable batteries. Herein, a capacity boost effect of Li- and Na-ion batteries was presented and clarified by nitrogen-doped graphene sheets. The reversible capacities progressively increased from 637.4 to 1050.4 mAh g^{-1} (164.8% increase) in Li-ion cell tests from 20 to 185 cycles, and from 187.3 to 247.5 mAh g^{-1} (132.1% increase) in Na-ion cell tests from 50 to 500 cycles. The mechanism of the capacity boost is proposed as an electrochemical induced cascading evolution of graphitic N to pyridinic and/or pyrrolic N, during which only these graphitic N adjacent pyridinic or pyrrolic structures can be taken precedence. The original and new generated pyridinic and pyrrolic N have strengthened binding energies to Li/Na atoms, thus increased the Li/Na coverage and delivered a progressive capacity boost with cycles until the entire favorable graphitic N transform into pyridinic and pyrrolic N.

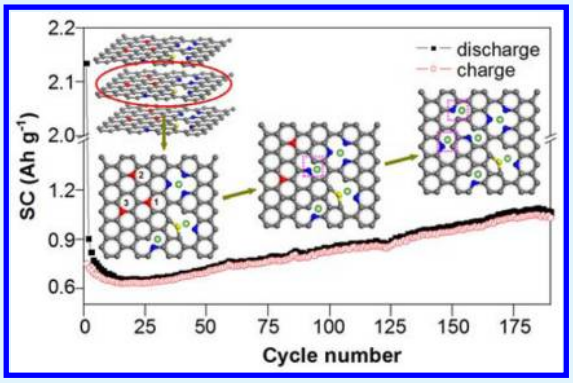

KEYWORDS: *nitrogen-doped graphene, cyclic performance, lithium ion battery, sodium ion battery, first-principles calculation, capacity boost*

INTRODUCTION

For developing advanced rechargeable batteries, the capacity and cyclic performance of electrode materials is particularly concerned.[1−3] Graphene and its derivatives have been intensively researched as a high-performance electrode material for both lithium-ion[3−10] and sodium-ion batteries.[11−14] Graphene sheets can increase the lithium and sodium storage capacities by ameliorating electrolyte infiltration and shortening the ion diffusion distance within active materials.[15−17] In spite of this, the lithium and sodium coverage on a single graphene layer leaves much than expected, because of the lower binding energies of lithium/sodium atoms to the graphene plane and the strong Coulombic repulsion of the lithium/sodium atoms on the opposite sides of the graphene sheet.[18−21] Consequently, heteroatom doping has been proposed to increase the binding of lithium and sodium to graphene layers.[22−26]

Nitrogen is one of the most attractive such dopants because its electronegativity (3.04) is higher than that of carbon (2.55) and its atomic diameter (71 pm) is close to that of carbon (75 pm).[27−29] The nitrogen atoms doped in graphene lattice are mainly formed as pyridinic, pyrrolic, and graphitic structures.[3,30−33] However, not all nitrogen-doped structures can improve the electrochemical capacities of graphene.[25,34−37] Theoretical results indicated that the pyridinic N and the pyrrolic N doped in graphene structures can strengthen the binding energies of lithium/sodium to the graphene layer and thus increase the lithium/sodium coverage, whereas the graphitic N doped in graphene structures can weaken the lithium/sodium binding and is not desirable for lithium/sodium storage.[14,25,35,36] In our previous work,[3] we developed a facile bottom-up strategy to fabricate high-concentration nitrogen-doped graphene (NDG) sheets, the nitrogen dopants in graphene sheets were determined to be pyridinic N, pyrrolic N, and graphitic N structures, and for electrochemical lithium storage, the NDG sheets displayed gradual capacity growth with charge−discharge cycling. The interesting phenomenon of capacity boost with cycles has been widely reported for transition metal oxides, and the increase of interfacial capacitive capacity with electrochemical cycles is generally understanded.[2,9,38−40] The effect of capacity boost was also reported for carbonaceous materials and it is ascribed to the defects proliferation of materials during electrochemical cycling.[23,41,42]

Received: June 21, 2016
Accepted: September 16, 2016
Published: September 16, 2016

DOI: 10.1021/acsami.6b07390
ACS Appl. Mater. Interfaces 2016, 8, 26722−26729

In this work, NDG electrodes were investigated for lithium and sodium storage, the long-term cyclic performance was determined, and the structural evolution of the NDG was investigated by ex situ X-ray photoelectron spectroscopy combined with first-principles calculations. It was found that the graphitic N in NDG sheets can gradually transform into pyridinic N and/or pyrrolic N structures during charge−discharge cycling, thus increasing the Li/Na coverage of NDG sheet and exhibited a cascading capacity boost effect during the initial hundred cycles until all graphitic N with the favorable structures of adjacent pyridinic N and pyrrolic N transform into pyridinic N and pyrrolic N.

METHODS

Synthesis of NDG. Dicyandiamide (99.5%) and monohydrate glucose (analytically pure) were used without further purification. In a typical synthesis, Dicyandiamide (48 g) and monohydrate glucose (2.4 g) were completely dissolved in deionized water under vigorous stirring and then removed from the water. After drying, the obtained powder was enclosed in a tube furnace under an argon atmosphere, and was heated to 580 °C and preserved at this temperature for 4 h. The temperature was then raised to 850 °C and maintained at this temperature for 6 h. The NDG formed after cooling.[3]

Material Characterizations. Transmission electron microscopy (TEM) images were captured on a JEOL-2010 instrument at an acceleration voltage of 200 kV. Elemental mapping images of a single NDG sheet were scanned by energy filtered TEM (EFTEM) (JEM-ARM200F). The surface area and porosity were studied by standard nitrogen adsorption isotherms at 77 K using an automated Micropore gas analyzer ASAP 2020 (Micromeritics Instruments). Raman spectra were obtained with a high-resolution, dispersive Raman spectrometer system (Horiba-Jobin Yvon LabRam HR) equipped with a visible laser excitation of 514 nm. Further, the surface chemistries and the nitrogen doping structures of NDG were determined by X-ray photoelectron spectroscopy (XPS) (ESCALAB 250 Xi; Al anode X-ray source). The NDG electrodes after charge−discharge cycling for the XPS analysis were prepared by charging the electrodes to 3.0 V and equilibrating at that potential for 1 h to attain steady-state condition, then washing with dimethyl carbonate (DMC), drying, and transferring to the XPS apparatus with argon gas shielding. Argon-ion etching was used to obtain concentration-depth profiles of the NDG electrodes, which provided structural information on the solid-electrolyte interphase (SEI) and the NDG electrode.

Electrochemical Measurements. Working electrodes were prepared by spreading a mixture of NDG (70 wt %) and polyvinylidene fluoride (PVDF, 30 wt %, Kynar FLEX 900, Elf Atochem) dissolved in *N*-methylpyrrolidone (Fluka Inc., St. Louis, MO) onto a Cu foil (thickness: 20 μm) current collector. The mass loadings of active material in the working electrodes are 0.3−0.5 mg cm^{-2}. The electrolyte consisted of 1 M $LiPF_6$ in a mixture of isometric ethylene carbonate (EC), dimethyl carbonate (DMC), and diethyl carbonate for the Li-ion cell and 1 M $NaClO_4$ in a mixture of isometric EC and DMC for the Na-ion cell. The electrochemical characterizations were conducted in 2025-type coin cells using Li foil (99.9%, China Energy Lithium Co., Ltd., Tianjin) and Na foil (99.5%, Sinopharm Chemical Reagent, Co., Ltd., Shanghai) as the counter electrodes. The charge−discharge experiments were conducted on a battery testing system (Neware, Shenzhen) over a voltage range of 0.05−3 V. The reported specific capacities are all normalized to the weight of the active materials.

Theoretical Calculations. The first-principles calculations were performed by using the plane-wave projector-augmented wave method, as implemented in the Vienna ab initio simulation package (VASP). The electron−ion interactions were described by the projected augmented wave (PAW) method. To obtain reliable optimized structures, the maximum residual force was set to less than 0.001 eV/Å, energies were converged to within 1×10^{-5} eV per atom, and the *k*-point mesh was set to $7 \times 7 \times 1$ ($5 \times 5 \times 1$ supercell). The structural configurations were optimized through fully relaxing the atomic structures to minimize their total energies. To ensure the accuracy of the calculated results, an energy cutoff of 450 eV was used in all cases. A vacuum of 20 Å was set to isolate graphene sheets for reducing the interactions between each sheet. The exchange-correlation potential was calculated based on the local density approximation.

RESULTS AND DISCUSSION

The morphology of the NDG sheets was investigated by TEM, as shown in Figure 1. The NDG sheet displays a conspicuous

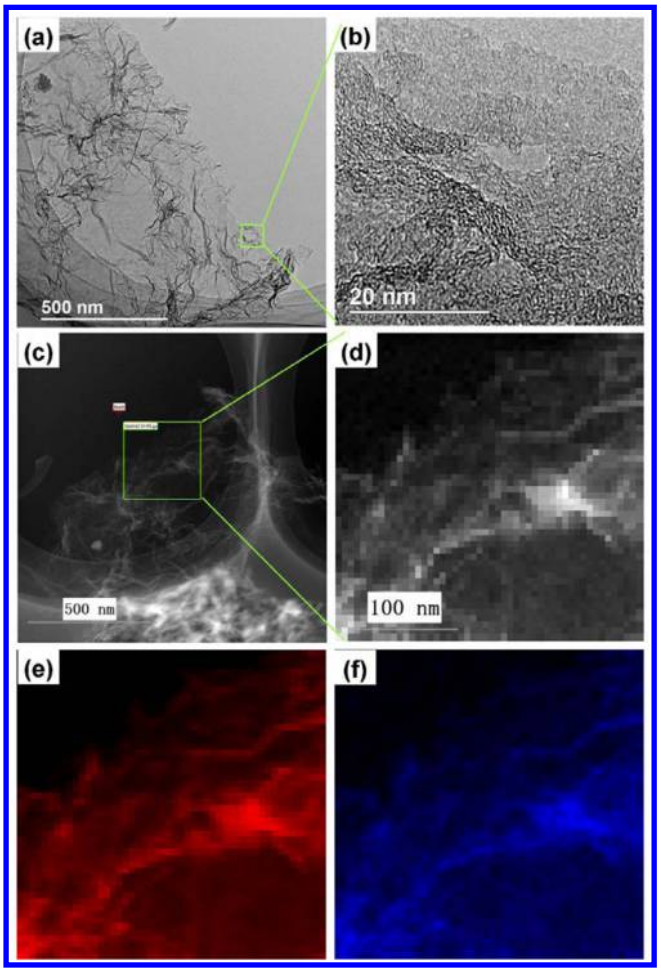

Figure 1. Elemental mapping of the NDG sheet: (a) TEM, (b) HRTEM, (c) survey image for EFTEM, (d) selected area low-loss EELS spectrum image, (e) C−K (279.0−331.5 eV) mapping, and (f) N−K (393.0−443.5 eV) mapping.

wrinkled appearance with homogeneous distribution of C and N elements. The wrinkle is common in graphene materials, which could be due to vertically aligning of graphene layers. For NDG, because of the different bond lengths of C−N and C−C bonds, and the interactions of lone pair electrons of the N atoms, there could be some inner stress in graphene layer, the stress could also lead to the twisting of graphene layer and generated additional out-of-plane wrinkles. The high resolution TEM (HRTEM) image (Figure 1b) reveals more disordered domains in the graphene sheet, which is an intrinsic feature of heteroatom doping of graphene materials.[3] Because of the much higher N doping degree (N content is 13.1% determined by XPS) of NDG in this work, there could be higher

DOI: 10.1021/acsami.6b07390
ACS Appl. Mater. Interfaces 2016, 8, 26722−26729

concentration of N defects and other imperfections in the graphene domains, and thus exhibited the lower crystallinity of NDG,[33] which can be confirmed by the XRD results (Figure S 1d). The broad D (1360 cm^{-1}), G (1580 cm^{-1}), and 2D (~2800 cm^{-1}) bands of Raman spectroscopy (Figure S1e) also confirm this disordered structure.[43−46] The intensity ratio of D to G is 2.47, indicating a considerable number of structure defects in NDG.[47] The type H3 hysteresis loop of nitrogen adsorption−desorption isotherm (Figure S1f), suggesting the slit-shaped pores between parallel graphene layers of NDG.[3,48] The calculated Brunauer-Emmett- Teller (BET) specific surface area of NDG is 398 m^2 g^{-1}, verified that the NDG are the few-layer graphene sheets. The lower crystallinity, more defects, and favorable porosity could enhance the interfacial process of NDG electrode with electrolyte and improved the diffusion of lithium/sodium ion between graphene layers, thus exhibiting a superior rate performance.[33]

The N content and structure of NDG could be optimized by changing the synthesis conditions (Supporting Information, section 1). XPS indicated that the C, N, and O atomic percentages of the NDG (Figure S1a and Table S1, sample-4) are 82.5%, 13.1%, and 4.4%, respectively. The sharp peak at binding energy of 284.6 eV could be resolved from the high-resolution XPS C 1s spectra (Figure S1b), illustrating the sp^2-hybridized graphitic carbon framework in NDG. The other peaks at higher band energies could be assigned to the oxygen- and/or nitrogen-containing groups attached to the aromatic ring of the graphene plane.[3,9,30,31,49] From the high-resolution N 1s spectra of NDG (Figure S1c, Table S5), the main N components could be resolved as pyridinic N (398.2 eV), pyrrolic N (400.5 eV), and graphitic N (401.2 eV), corresponding to the percentage of 54, 30, and 16%, respectively.[3,31,50−53] To systematically analyze the N structure of NDG, we uniformly used the same binding energy value for N 1s spectra deconvolution in the following sections.

The electrochemical charge−discharge performance of NDG electrode was investigated by galvanostatic charge−discharge cycling in Li- and Na-ion coin cells at current density of 100 mA g^{-1} over the voltage range of 0.05−3 V. As shown in Figure 2, the discharge/charge specific capacities of NDG electrodes are 2134.6/751.4 mAh g^{-1} in Li-ion half cells and 1349.6/375.4 mAh g^{-1} in Na-ion half cells, respectively. The large capacity losses in the first cycle are attributed mainly to excessive surface reactions on the SEI films;[3,16,17] irreversible discharge reactions at the graphitic nitrogen doping sites, or the other undesirable dopants which can cause large capacity loss.[34] As discussed earlier,[3] the discharge curves started from 3.0 V without distinct voltage plateaus, and the charge profiles displayed appreciable voltage hysteresis, indicating that the extraction of lithium/sodium ions from the slit-shaped micropores has to pass through graphene crystallites over the entire voltage range. The charge−discharge behavior of the NDG electrodes is further reflected in detail by the oxidation−reduction peaks in the differential capacity (DC) versus voltage (dQ/dV) plots in Figure 2c, d derived from the voltage profiles in Figure 2a, b inset. Although it exhibited similar charge−discharge behaviors, the differential capacities of the NDG electrode in Na-ion cell are far less than those in Li-ion cell, this is ascribed mainly to the larger size and poor bonding characteristics of sodium ions.[54] Especially worth noting is the specific capacity upturn with charge−discharge cycling (Figure 2e, f). It gradually increases from 637.4 (25th cycle) mAh g^{-1} to 1050.4 (185th cycle) mAh g^{-1} (164.8% increase) for the Li-ion cell and from

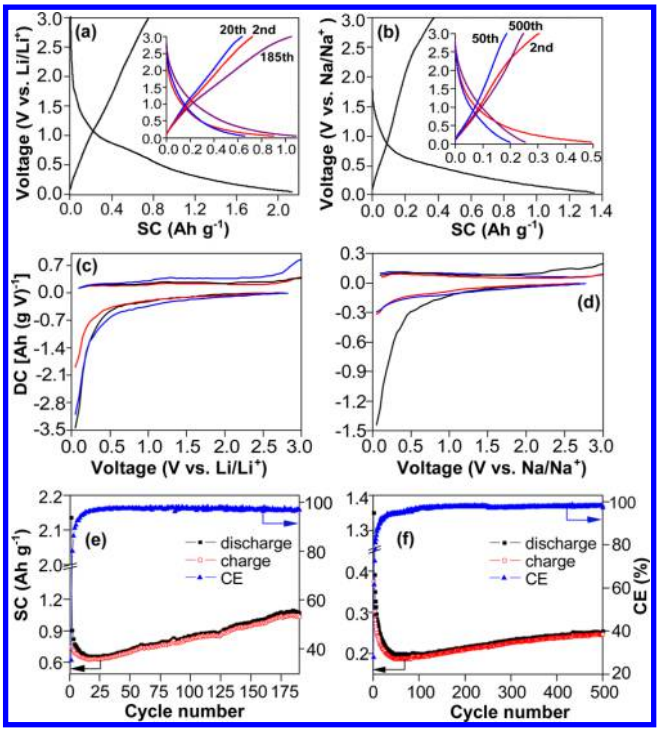

Figure 2. (a, b) Charge−discharge profiles of the first and (inset) the following cycles, (c, d) corresponding charge−discharge dQ/dV plots, and (e, f) cyclic performance of NDG electrodes in (a, c, e) Li-ion and (b, d, f) Na-ion half cells at current density of 100 mA g^{-1} over the voltage range of 0.05−3 V. SC and CE denote specific capacity and Coulombic efficiency, respectively.

187.3 (50th cycle) mAh g^{-1} to 247.5 (500th cycle) mAh g^{-1} (132.1% increase) for the Na-ion cell. When cycling in even longer term (at current density 1 A g^{-1}), the appearance of gradual capacity boost terminates after 300 cycles, and then the capacity can be maintained in the follow cycling (Figure S6).

To further survey this striking phenomenon of capacity boost, the NDG electrodes after cycling were investigated by ex situ XPS. The cycled NDG electrodes were washed with DMC and etched with argon ions to scratch the SEI layers. The real time XPS spectra were collected at various etching time, we monitored the N content to ascertaining the exposing of active materials. The concentration-depth XPS spectra showed that there are extraneous C 1s and O 1s information on PVDF binder and SEI layers, but the N 1s spectra presented simpler signal only about the NDG active materials (Supporting Information, section 4). At the beginning of etching, the N element of the cycled NDG electrode of the Li-ion cell cannot be detected until the etching time is up to 380 s (Table S3), indicating that there is not any N-containing component in the SEI layers, and the NDG is well-coated by SEI layer. When etched 380 s, the N element was detected for the first time with the percentage of 0.65%, which then increases up to 1.38% in the further etching. Compare with that of the fresh NDG electrode, the XPS C 1s results of cycled NDG (Figure 3c, e) reveal the much more nonaromatic C components (285.7−291.4 eV), indicated there is still some SEI layer covered on the NDG even after 380 s etching (for Li-ion cell, and it is 280 s etching for Na-ion cell). Whereas the partly exposed NDG could not be seriously affected, therefore, the XPS N 1s results at these etching levels (380 s etching for cycled in Li-ion cell, and 280 s etching for cycled in Na-ion cell) can be used for

DOI: 10.1021/acsami.6b07390
ACS Appl. Mater. Interfaces 2016, 8, 26722−26729

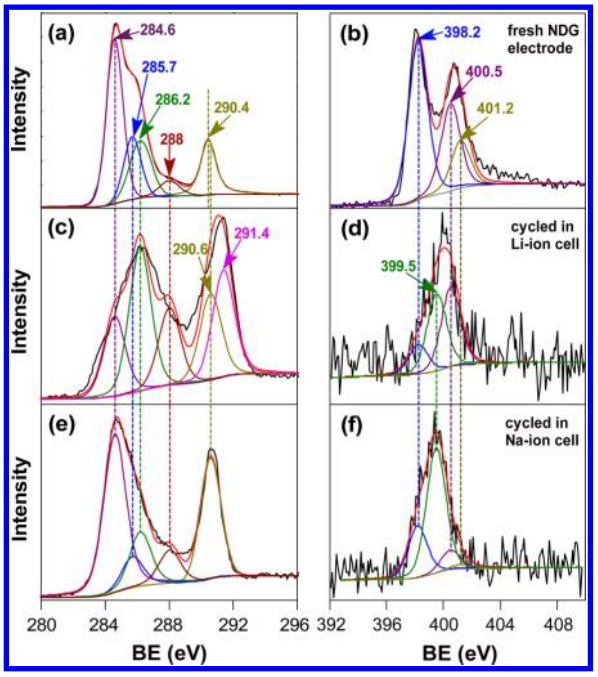

Figure 3. High-resolution (left panels) C 1s and (right panels) N 1s XPS results of (a, b) fresh NDG electrode and of the NDG electrodes after cycled in (c, d) Li-ion cell (etching 380 s) and (e, f) Na-ion cell (etching 280 s). BE denotes the binding energy.

analyzing the structure evolution of NDG electrode. As shown in Figures 3, the XPS peaks ascribing to the pyridinic N (398.2 eV) and pyrrolic N (400.5 eV) can be deconvoluted from the N 1s spectra of cycled NDG electrode.[3,31] Besides, a new peak at 399.5 eV is also deconvoluted, which could be ascribed to the Li/Na protonized pyridinic N structures.[50−53,55] Most noticeably, the peak corresponding to graphitic N (401.2 eV) cannot be identified almost from the N 1s spectra of NDG electrode after cycled in ether the Li- or Na-ion cells, whereas there is not any other N-containing component in the testing-cells or the SEI layers except the NDG, and thus the total N content of NDG could not change. Therefore, we conclude that the graphitic N of NDG could transform into pyridinic or pyrrolic N structures during the electrochemical cycling.

Theoretical calculations were also employed to study the structural evolution of NDG. We surveyed the lithium adsorption in the NDG sheet by first-principles calculations, the structural models of pristine graphene (PG), pyridinic NDG (PIG), pyrrolic NDG (PRG), and graphitic NDG (GG) were constructed according to the experimental results and literatures.[14,24,56] The particular situation of GG adjacent to lithiated PIG (Li-GG) was also considered. A single lithium atom was added to the different structural models, and the optimal lithium storage sites were determined by theoretical calculations. As shown in Figure 4, from the side view, the lithium atoms are adsorbed out of the graphene plane for all models; from the top view, the lithium atoms are at the center sites of a hollow or defect in the symmetrical structures but diverge from the center in the asymmetrical structures, whether nitrogen doping or not. The average adsorption energy (E_{ad}) can reveal more detailed interactions of the Li atom to graphene sheet, which is given by the formula

$$E_{ad} = E_{Li-NDG} - (E_{Li} + E_{NDG}) \quad (1)$$

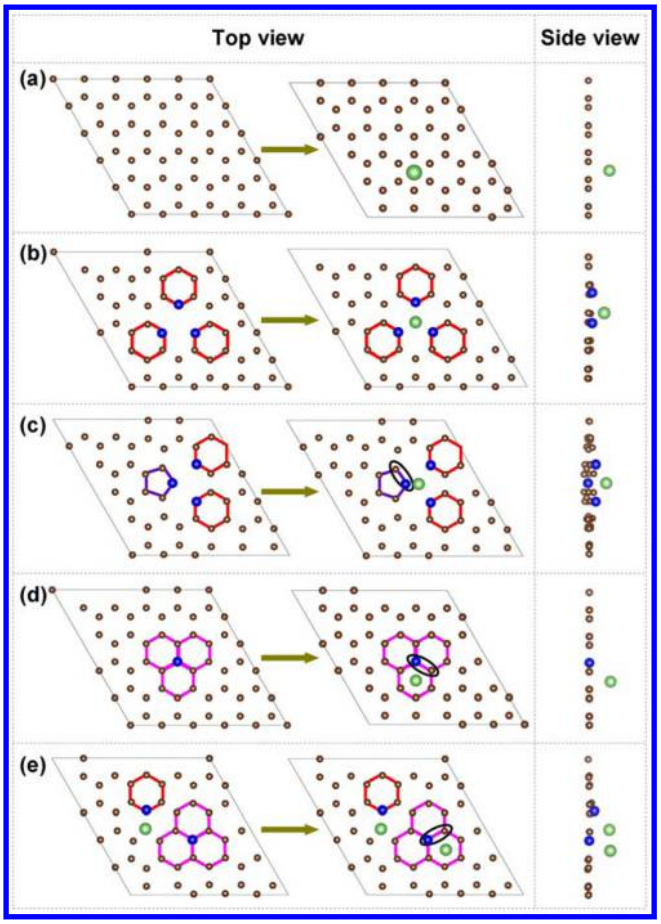

Figure 4. Most stable lithium storage sites in (a) PG, (b) PIG, (c) PRG, (d) GG, and (e) Li-GG. The brown, blue, and green spheres denote carbon, nitrogen, and lithium atoms, respectively. The C−N bonds with the biggest change in asymmetric structure are marked with black circles, and the corresponding bond length change data are presented in Table 1.

Where E_{Li}, E_{NDG}, and E_{Li-NDG} are the total energies of the isolated Li atom, the nitrogen doped structural model, and the Li-graphene interacting system, respectively. The more negative E_{ad} means a stronger binding interaction between lithium atom and the graphene plane. Calculations of the E_{ad}, shown in Table 1, indicate that PIG is the most suitable for lithium storage, PRG is the second best, PG is the third, but the GG and Li-GG show much poorer lithium-storage ability. These results are

Table 1. Most Stable Site, Average Adsorption Energy (E_{ad}), and Biggest Change in C−N Bond Length (Δ_{BL}) after a Single Lithium Atom Adsorbed in Different Models of Graphene Sheet

structure	most stable site	E_{ad} (eV)	Δ_{BL} (pm)
PG	center of hollow site	−1.65	0.9 (C−C)
PIG	center of defect	−5.30	1.1
PRG	defect site, near pyrrolic nitrogen atom	−4.58	−0.5
GG	hollow site, away from graphitic nitrogen atom	−1.20	2.1
Li-GG	hollow site, away from graphitic nitrogen atom	−1.22	3.5

[a]The C and N atoms are marked with black circles on the corresponding structure model in Figure 4.

DOI: 10.1021/acsami.6b07390
ACS Appl. Mater. Interfaces 2016, 8, 26722−26729

consistent with the literature.[24,36,56] Furthermore, the data in Table 1 revealed that the C−N bond was stretched (Δ_{BL} = 2.1 pm) when a lithium ions was put in GG, and this stretching became even larger in Li-GG (Δ_{BL} = 3.5 pm). To understand the interaction mechanism and hybridization degree of C−N bonds, the partial density of states (PDOS) with p_x and p_y orbitals of C and N from GG and Li-GG without Li atom absorption at GG site (left panel in Figure 4d, e) are calculated and shown in Figure 5. The p_x and p_y orbitals of N in GG are

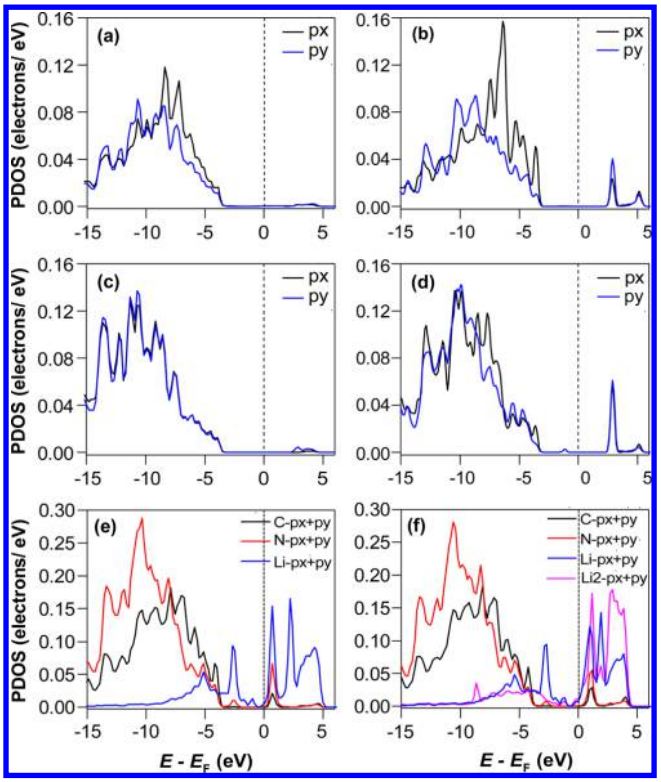

Figure 5. PDOS: The *px*, *py* orbitals of (a, (b) C and (c, d) N atoms in (a, c) GG and (b, d) Li-GG without Li atom; the *px* + *py* orbitals of C, N, and Li atoms in Li-GG (e) before and (f) after adsorbing another Li atom. The C and N atoms are marked with black circles on the corresponding structure model in Figure 4. The dashed line at zero eV indicates the Fermi level.

almost the same while these orbitals for GG-type N are evidently different in Li-GG without Li atom. The differences of the p_x and p_y orbitals of C are more obvious for the peaks of p_x and p_y orbitals, which are staggered in Li-GG. These changes illustrate that C−N bonds are deviated from sp2 bonding in Li-GG. Bader charge analysis can give quantitative results of charge on C and N atoms. As listed in Table 2, for all structures, the GG-type N atom is quite negative, with a charge of about 1.2 *e*, because N is a radical and more electronegative than C. We notice that C bonded with GG-type N shows negative charge in Li-GG absorbed a Li atom while it shows positive in other structures, i.e., in Li-GG, after absorbing a Li atom at GG site, the Coulomb force between the adjacent C and N changes from attraction to repulsion, which is consistent with the enlarged C−N bond length. Thus, the C−N bonds of GG structure of NDG could be weakened due to lithium/sodium atom adsorption during electrochemical cycling,[36] indicating the easier process for C−N bond broken and transformed into PIG and/or PRG, which supports the experimental XPS observation that the structure of graphitic N evolves to pyridinic N and pyrrolic N during the electrochemical cycling. Because the stretching of C−N bonds are much larger (by a factor of 67%) for GG structures adjacent to lithiated PIG than those not adjacent to lithiated PIG, we can conclude that this transformation occurs preferentially at the GG structures adjacent to the PIG. This conclusion is reasonable because the defected PIG site can release the stress induced by the stretched C−N bonds of GG structures more conveniently, thus leading to more enlarged C−N bonds of GG structure adjacent to it. As discussed above, the GG is electronically sufficient and cannot contribute to the lithium/sodium storage capacities, whereas the PIG and the PRG structures can increase the lithium/sodium coverage in the graphene layers and generate more capacity for both lithium and sodium storage. After the entire graphitic N with favorable structures transformed into pyridinic N or pyrrolic N, the NDG could delivered the maximum capacity and then maintained it during the subsequent cycling (Figures S6 and S7).

According to these results, we proposed a model to explain the capacity boost for NDG sheets. As shown in Figure 6, the

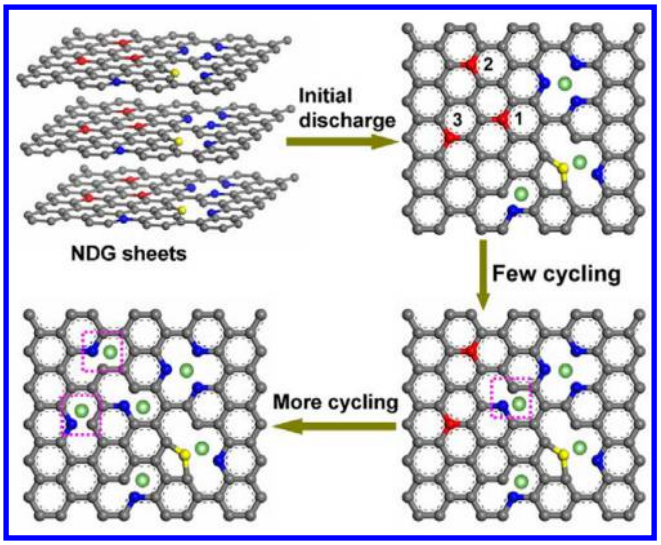

Figure 6. Schematic illustration for the capacity boosting of NDG sheets during charge−discharge cycling. The gray, blue, yellow, red, and green spheres denote C, pyridinic N, pyrrolic N, graphitic N, and Li/Na atoms, respectively; the new added storage sites in each stage are marked with pink squares.

Table 2. Bader Charges on N and C Atoms in GG and Li-GG Model before and after a Li Atom Adsorbed

	GG (e)			Li-GG (e)		
atom	before	after	change	before	after	change
N	−1.2381	−1.2641	−0.026	−1.1744	−1.1339	0.0405
C	0.0537	0.1661	0.1124	0.1811	−0.0126	−0.1937

[a]The C and N atoms are marked with black circles on the corresponding structure model in Figure 4.

DOI: 10.1021/acsami.6b07390
ACS Appl. Mater. Interfaces 2016, 8, 26722−26729

pyridinic N, pyrrolic N, and graphitic N structures in a single graphene layer of NDG sheets were marked with blue, yellow, and red spheres, respectively. For the initial discharge, the lithium/sodium atoms could perch on the PIG and PRG sites. After several cycles, the graphitic N (GG-1) adjacent to PIG structures broken and transformed into a PIG structure, and generated a new storage site. During another follow cycles, the graphitic N (GG-2 and GG-3) gone through the evolution process as GG-1, and generated another two storage sites. During long-term electrochemical cycling, the GG with different surrounding structures could progressively transform in to PIG or PRG, and thus delivered a cascading capacity boost effect. After all of the graphitic N atoms with favorable structures have transformed into pyridinic N and/or pyrrolic N, the NDG electrode can achieve the maximum capacity and maintained it during the subsequent cycling.

CONCLUSIONS

In summary, nitrogen-doped graphene sheets with three types of N structures (pyridinic N, pyrrolic N and graphitic N) were investigated for lithium and sodium storage, the prominent appearance of gradual capacity increase during long-term charge−discharge cycling displayed. The reversible lithium and sodium storage capacities increased from 637.4 to 1050.4 mAh g^{-1} (164.8% increase) over 20 to 185 cycles, and from 187.3 to 247.5 mAh g^{-1} (132.1% increase) from 50 to 500 cycles, respectively. By ex situ XPS combine with first-principles calculations, the capacity boost is confirmed to the cascading evolution of graphitic N to pyridinic N and/or pyrrolic N. The evolution is mostly affected by the adjacent structures (especially the pyridinic N) of the graphitic N, the original and new generated N structures are posited to have strengthened the binding energies of Li/Na atoms to graphene sheet, thus increased the Li/Na coverage of NDG sheet and delivered a progressive capacity boost during the initial hundred cycles. This capacity boost of NDG is continued until all of the graphitic N with favorable structures transformed into pyridinic N and/or pyrrolic N. This work confirmed the electrochemical induced N structure evolution of NDG sheets, which provide a good deal of insight into the capacity boost of NDG electrode, and it may also present a fresh perspective for using nitrogen-doped graphene materials in various applications beyond batteries.

ASSOCIATED CONTENT

Supporting Information

This material is available free of charge on the Internet at The Supporting Information is available free of charge on the ACS Publications website at DOI: 10.1021/acsami.6b07390.

Rate performance of the NDG electrode; supplementary characterization results and discussions (PDF)

AUTHOR INFORMATION

Corresponding Authors

*E-mail: panfeng@pkusz.edu.cn.
*E-mail: zhuangquanchao@126.com.
*E-mail: zhengjx@pkusz.edu.cn.

Author Contributions

†L.-L.T. and S.-B.L. contributed equally to this work. L.L.T. conceived, designed, and carried out the experiment and analyzed the data. S.B.L. and J.X.Z. preformed the theoretical calculations. All authors discussed the results and commented on the manuscript.

Notes

The authors declare no competing financial interest.

ACKNOWLEDGMENTS

The authors acknowledge financial support from the Fund from the National Project for EV Batteries (20121110, Optimum Nano, Shenzhen), the Guangdong Innovation Team Project (2013N080), and the Shenzhen Science and Technology Research Grant (ZDSY20130331145131323, CXZZ20120829172325895, and JCYJ20150629144526408). Argonne National Laboratory, a U.S. Department of Energy Office of Science laboratory, is operated under Contract DE-AC02-06CH11357. The authors are also grateful to Dr. Hai-Biao Chen and Dr. Yi-Dong Liu for helpful discussions about BET and XPS results.

REFERENCES

(1) Choi, N. S.; Chen, Z. H.; Freunberger, S. A.; Ji, X. L.; Sun, Y. K.; Amine, K.; Yushin, G.; Nazar, L. F.; Cho, J.; Bruce, P. G. Challenges Facing Lithium Batteries and Electrical Double-Layer Capacitors. *Angew. Chem., Int. Ed.* **2012**, *51*, 9994−10024.

(2) Sun, H. T.; Xin, G. Q.; Hu, T.; Yu, M. P.; Shao, D. L.; Sun, X.; Lian, J. High-Rate Lithiation-Induced Reactivation of Mesoporous Hollow Spheres for Long-Lived Lithium-Ion Batteries. *Nat. Commun.* **2014**, *5*, 4526.

(3) Tian, L. L.; Wei, X. Y.; Zhuang, Q. C.; Jiang, C. H.; Wu, C.; Ma, G. Y.; Zhao, X.; Zong, Z. M.; Sun, S. G. Bottom-Up Synthesis of Nitrogen-Doped Graphene Sheets for Ultrafast Lithium Storage. *Nanoscale* **2014**, *6*, 6075−6083.

(4) Raccichini, R.; Varzi, A.; Passerini, S.; Scrosati, B. The Role of Graphene for Electrochemical Energy Storage. *Nat. Mater.* **2015**, *14*, 271−279.

(5) Wang, G. X.; Shen, X. P.; Yao, J.; Park, J. Graphene Nanosheets for Enhanced Lithium Storage in Lithium Ion Batteries. *Carbon* **2009**, *47*, 2049−2053.

(6) Yoo, E.; Kim, J.; Hosono, E.; Zhou, H.; Kudo, T.; Honma, I. Large Reversible Li Storage of Graphene Nanosheet Families for Use in Rechargeable Lithium Ion Batteries. *Nano Lett.* **2008**, *8*, 2277−2282.

(7) Zhao, X.; Hayner, C. M.; Kung, M. C.; Kung, H. H. Flexible Holey Graphene Paper Electrodes with Enhanced Rate Capability for Energy Storage Applications. *ACS Nano* **2011**, *5*, 8739−8749.

(8) Wu, Z.-S.; Zhou, G.; Yin, L.-C.; Ren, W.; Li, F.; Cheng, H.-M. Graphene/Metal Oxide Composite Electrode Materials for Energy Storage. *Nano Energy* **2012**, *1*, 107−131.

(9) Tian, L.; Zhuang, Q.; Li, J.; Wu, C.; Shi, Y.; Sun, S. The Production of Self-Assembled Fe_2O_3-Graphene Hybrid Materials by a Hydrothermal Process for Improved Li-Cycling. *Electrochim. Acta* **2012**, *65*, 153−158.

(10) Jaber-Ansari, L.; Puntambekar, K. P.; Tavassol, H.; Yildirim, H.; Kinaci, A.; Kumar, R.; Saldana, S. J.; Gewirth, A. A.; Greeley, J. P.; Chan, M. K. Y.; Hersam, M. C. Defect Evolution in Graphene upon Electrochemical Lithiation. *ACS Appl. Mater. Interfaces* **2014**, *6*, 17626−17636.

(11) Xu, J. T.; Wang, M.; Wickramaratne, N. P.; Jaroniec, M.; Dou, S. X.; Dai, L. M. High-Performance Sodium Ion Batteries Based on a 3D Anode from Nitrogen-Doped Graphene Foams. *Adv. Mater.* **2015**, *27*, 2042−2048.

(12) Kim, H.; Park, Y. U.; Park, K. Y.; Lim, H. D.; Hong, J.; Kang, K. Novel Transition-Metal-Free Cathode for High Energy and Power Sodium Rechargeable Batteries. *Nano Energy* **2014**, *4*, 97−104.

(13) Datta, D.; Li, J. W.; Shenoy, V. B. Defective Graphene as a High-Capacity Anode Material for Na- and Ca-Ion Batteries. *ACS Appl. Mater. Interfaces* **2014**, *6*, 1788−1795.

DOI: 10.1021/acsami.6b07390
ACS Appl. Mater. Interfaces 2016, 8, 26722−26729

(14) Shen, H.; Rao, D. W.; Xi, X. M.; Liu, Y. Z.; Shen, X. Q. N-Substituted Defective Graphene Sheets: Promising Electrode Materials for Na-Ion Batteries. *RSC Adv.* **2015**, *5*, 17042−17048.
(15) Kaskhedikar, N. A.; Maier, J. Lithium Storage in Carbon Nanostructures. *Adv. Mater.* **2009**, *21*, 2664−2680.
(16) Pan, D.; Wang, S.; Zhao, B.; Wu, M.; Zhang, H.; Wang, Y.; Jiao, Z. Li Storage Properties of Disordered Graphene Nanosheets. *Chem. Mater.* **2009**, *21*, 3136−3142.
(17) Tian, L.; Zhuang, Q.; Li, J.; Shi, Y.; Chen, J.; Lu, F.; Sun, S. Mechanism of Intercalation and Deintercalation of Lithium Ions in Graphene Nanosheets. *Chin. Sci. Bull.* **2011**, *56*, 3204−3212.
(18) Pollak, E.; Geng, B.; Jeon, K.-J.; Lucas, I. T.; Richardson, T. J.; Wang, F.; Kostecki, R. The Interaction of Li^+ with Single-Layer and Few-Layer Graphene. *Nano Lett.* **2010**, *10*, 3386−3388.
(19) Ferre-Vilaplana, A. Storage of Hydrogen Adsorbed on Alkali Metal Doped Single-Layer All-Carbon Materials. *J. Phys. Chem. C* **2008**, *112*, 3998−4004.
(20) Ataca, C.; Akturk, E.; Ciraci, S.; Ustunel, H. High-Capacity Hydrogen Storage by Metallized Graphene. *Appl. Phys. Lett.* **2008**, *93*, 043123.
(21) Lee, E.; Persson, K. A. Li Absorption and Intercalation in Single Layer Graphene and Few Layer Graphene by First Principles. *Nano Lett.* **2012**, *12*, 4624−4628.
(22) Wu, Z.-S.; Ren, W.; Xu, L.; Li, F.; Cheng, H.-M. Doped Graphene Sheets as Anode Materials with Superhigh Rate and Large Capacity for Lithium Ion Batteries. *ACS Nano* **2011**, *5*, 5463−5471.
(23) Lee, J. S.; Park, G. S.; Lee, H. I.; Kim, S. T.; Cao, R. G.; Liu, M. L.; Cho, J. Ketjenblack Carbon Supported Amorphous Manganese Oxides Nanowires as Highly Efficient Electrocatalyst for Oxygen Reduction Reaction in Alkaline Solutions. *Nano Lett.* **2011**, *11*, 5362−5366.
(24) Ma, C.; Shao, X.; Cao, D. Nitrogen-Doped Graphene Nanosheets as Anode Materials for Lithium Ion Batteries: A First-Principles Study. *J. Mater. Chem.* **2012**, *22*, 8911−8915.
(25) Kong, X. K.; Chen, Q. W. Improved Performance of Graphene Doped with Pyridinic N for Li-Ion Battery: A Density Functional Theory Model. *Phys. Chem. Chem. Phys.* **2013**, *15*, 12982−12987.
(26) Ling, C.; Mizuno, F. Boron-Doped Graphene as a Promising Anode for Na-Ion Batteries. *Phys. Chem. Chem. Phys.* **2014**, *16*, 10419−10424.
(27) Panchakarla, L. S.; Subrahmanyam, K. S.; Saha, S. K.; Govindaraj, A.; Krishnamurthy, H. R.; Waghmare, U. V.; Rao, C. N. R. Synthesis, Structure, and Properties of Boron- and Nitrogen-Doped Graphene. *Adv. Mater.* **2009**, *21*, 4726−4730.
(28) Jin, Z.; Yao, J.; Kittrell, C.; Tour, J. M. Large-Scale Growth and Characterizations of Nitrogen-Doped Monolayer Graphene Sheets. *ACS Nano* **2011**, *5*, 4112−4117.
(29) Pyykko, P.; Atsumi, M. Molecular Single-Bond Covalent Radii for Elements 1−118. *Chem. - Eur. J.* **2009**, *15*, 186−197.
(30) Reddy, A. L. M.; Srivastava, A.; Gowda, S. R.; Gullapalli, H.; Dubey, M.; Ajayan, P. M. Synthesis of Nitrogen-Doped Graphene Films for Lithium Battery Application. *ACS Nano* **2010**, *4*, 6337−6342.
(31) Wang, H.; Zhang, C.; Liu, Z.; Wang, L.; Han, P.; Xu, H.; Zhang, K.; Dong, S.; Yao, J.; Cui, G. Nitrogen-Doped Graphene Nanosheets with Excellent Lithium Storage Properties. *J. Mater. Chem.* **2011**, *21*, 5430−5434.
(32) Zheng, F. C.; Yang, Y.; Chen, Q. W. High Lithium Anodic Performance of Highly Nitrogen-Doped Porous Carbon Prepared from a Metal-Organic Framework. *Nat. Commun.* **2014**, *5*, 5261.
(33) Wang, X.; Weng, Q. H.; Liu, X. Z.; Wang, X. B.; Tang, D. M.; Tian, W.; Zhang, C.; Yi, W.; Liu, D. Q.; Bando, Y.; Golberg, D. Atomistic Origins of High Rate Capability and Capacity of N-Doped Graphene for Lithium Storage. *Nano Lett.* **2014**, *14*, 1164−1171.
(34) Veith, G. M.; Baggetto, L.; Adamczyk, L. A.; Guo, B.; Brown, S. S.; Sun, X.-G.; Albert, A. A.; Humble, J. R.; Barnes, C. E.; Bojdys, M. J.; Dai, S.; Dudney, N. J. Electrochemical and Solid-State Lithiation of Graphitic C_3N_4. *Chem. Mater.* **2013**, *25*, 503−508.
(35) Yu, Y.-X. Can All Nitrogen-Doped Defects Improve The Performance of Graphene Anode Materials for Lithium-Ion Batteries? *Phys. Chem. Chem. Phys.* **2013**, *15*, 16819−16827.
(36) Hankel, M.; Ye, D. L.; Wang, L. Z.; Searles, D. J. Lithium and Sodium Storage on Graphitic Carbon Nitride. *J. Phys. Chem. C* **2015**, *119*, 21921−21927.
(37) Liu, Y. Y.; Artyukhov, V. I.; Liu, M. J.; Harutyunyan, A. R.; Yakobson, B. I. Feasibility of Lithium Storage on Graphene and Its Derivatives. *J. Phys. Chem. Lett.* **2013**, *4*, 1737−1742.
(38) Tian, L.-L.; Zhang, M.-J.; Wu, C.; Wei, Y.; Zheng, J.-X.; Lin, L.-P.; Lu, J.; Amine, K.; Zhuang, Q.-C.; Pan, F. γ-Fe_2O_3 Nano-Crystalline Microspheres with Hybrid Behavior of Battery-Supercapacitor for Superior Lithium Storage. *ACS Appl. Mater. Interfaces* **2015**, *7*, 26284−26298.
(39) Zhukovskii, Y. F.; Kotomin, E. A.; Balaya, P.; Maier, J. Enhanced Interfacial Lithium Storage in Nanocomposites of Transition Metals with LiF And Li_2O: Comparison of DFT Calculations and Experimental Studies. *Solid State Sci.* **2008**, *10*, 491−495.
(40) Jamnik, J.; Maier, J. Nanocrystallinity Effects in Lithium Battery Materials- Aspects of Nano-Ionics. Part IV. *Phys. Chem. Chem. Phys.* **2003**, *5*, 5215−5220.
(41) Shin, W. H.; Jeong, H. M.; Kim, B. G.; Kang, J. K.; Choi, J. W. Nitrogen-Doped Multiwall Carbon Nanotubes for Lithium Storage with Extremely High Capacity. *Nano Lett.* **2012**, *12*, 2283−2288.
(42) Mukherjee, R.; Thomas, A. V.; Datta, D.; Singh, E.; Li, J. W.; Eksik, O.; Shenoy, V. B.; Koratkar, N. Defect-Induced Plating of Lithium Metal within Porous Graphene Networks. *Nat. Commun.* **2014**, *5*, 3710.
(43) Zheng, Z. M.; Wang, Y.; Zhang, A.; Zhang, T. R.; Cheng, F. Y.; Tao, Z. L.; Chen, J. Porous Li_2FeSiO_4/C Nanocomposite as The Cathode Material of Lithium-Ion Batteries. *J. Power Sources* **2012**, *198*, 229−235.
(44) Gonzalez-Gaitan, C.; Ruiz-Rosas, R.; Morallon, E.; Cazorla-Amoros, D. Functionalization of Carbon Nanotubes Using Amino-benzene Acids and Electrochemical Methods. Electroactivity for the Oxygen Reduction Reaction. *Int. J. Hydrogen Energy* **2015**, *40*, 11242−11253.
(45) Li, X.-H.; Kurasch, S.; Kaiser, U.; Antonietti, M. Synthesis of Monolayer-Patched Graphene from Glucose. *Angew. Chem., Int. Ed.* **2012**, *51*, 9689−9692.
(46) Sun, J.; Liu, H.; Chen, X.; Evans, D. G.; Yang, W.; Duan, X. Synthesis of Graphene Nanosheets with Good Control over The Number of Layers within The Two-Dimensional Galleries of Layered Double Hydroxides. *Chem. Commun.* **2012**, *48*, 8126−8128.
(47) Tian, L.-L.; Wei, X.-Y.; Zhuang, Q.-C.; Wu, C.; Xie, R.-L.; Zong, Z.-M.; Cui, Y.-L.; Sun, S.-G. Chiseled Nickel Hydroxide Nanoplates Growth on Graphene Sheets for Lithium Ion Batteries. *Nano* **2013**, *8*, 1350068.
(48) Luo, Z.; Lim, S.; Tian, Z.; Shang, J.; Lai, L.; MacDonald, B.; Fu, C.; Shen, Z.; Yu, T.; Lin, J. Pyridinic N Doped Graphene: Synthesis, Electronic Structure, and Electrocatalytic Property. *J. Mater. Chem.* **2011**, *21*, 8038−8044.
(49) Lian, P.; Zhu, X.; Liang, S.; Li, Z.; Yang, W.; Wang, H. Large Reversible Capacity of High Quality Graphene Sheets as an Anode Material for Lithium-Ion Batteries. *Electrochim. Acta* **2010**, *55*, 3909−3914.
(50) Pels, J. R.; Kapteijn, F.; Moulijn, J. A.; Zhu, Q.; Thomas, K. M. Evolution of Nitrogen Functionalities in Carbonaceous Materials during Pyrolysis. *Carbon* **1995**, *33*, 1641−1653.
(51) Song, J.; Xu, T.; Gordin, M. L.; Zhu, P.; Lv, D.; Jiang, Y.-B.; Chen, Y.; Duan, Y.; Wang, D. Nitrogen-Doped Mesoporous Carbon Promoted Chemical Adsorption of Sulfur and Fabrication of High-Areal- Capacity Sulfur Cathode with Exceptional Cycling Stability for Lithium- Sulfur Batteries. *Adv. Funct. Mater.* **2014**, *24*, 1243−1250.
(52) Bian, S.-W.; Ma, Z.; Song, W.-G. Preparation and Characterization of Carbon Nitride Nanotubes and Their Applications as Catalyst Supporter. *J. Phys. Chem. C* **2009**, *113*, 8668−8672.
(53) Cui, Y.; Zhang, J.; Zhang, G.; Huang, J.; Liu, P.; Antonietti, M.; Wang, X. Synthesis of Bulk and Nanoporous Carbon Nitride Polymers

DOI: 10.1021/acsami.6b07390
ACS Appl. Mater. Interfaces 2016, 8, 26722−26729

from Ammonium Thiocyanate for Photocatalytic Hydrogen Evolution. *J. Mater. Chem.* **2011**, *21*, 13032−13039.
(54) Hong, S. Y.; Kim, Y.; Park, Y.; Choi, A.; Choi, N. S.; Lee, K. T. Charge Carriers in Rechargeable Batteries: Na Ions vs. Li Ions. *Energy Environ. Sci.* **2013**, *6*, 2067−2081.
(55) Li, X. L.; Wang, H. L.; Robinson, J. T.; Sanchez, H.; Diankov, G.; Dai, H. J. Simultaneous Nitrogen Doping and Reduction of Graphene Oxide. *J. Am. Chem. Soc.* **2009**, *131*, 15939−15944.
(56) Jing, Y.; Zhou, Z. Computational Insights into Oxygen Reduction Reaction and Initial Li_2O_2 Nucleation on Pristine and N-Doped Graphene in Li-O_2 Batteries. *ACS Catal.* **2015**, *5*, 4309−4317.

DOI: 10.1021/acsami.6b07390
ACS Appl. Mater. Interfaces 2016, 8, 26722−26729